J Solid State Electrochem (2012) 16:953–962
DOI 10.1007/s10008-011-1469-6

ORIGINAL PAPER

A facile carbothermal preparation of Sn–Co–C composite electrodes for Li-ion batteries using low-cost carbons

Francisco Nacimiento · Pedro Lavela · José Luis Tirado · Juan Miguel Jiménez-Mateos

Received: 9 May 2011 / Revised: 7 June 2011 / Accepted: 8 June 2011 / Published online: 18 June 2011

Abstract Sn–Co–C composites were prepared by carbothermal reaction of ball-milled precursors. X-ray diffraction and ^{119}Sn Mössbauer spectroscopy of the original composites revealed the predominance of Sn and $CoSn_2$ phases for those samples prepared with a high Sn/Co ratio. Electron microscopy images showed a homogeneous dispersion of sub-micrometric metallic particles in the carbon matrix. Galvanostatic cycling at several kinetic rates revealed that $Sn_7Co_1C_{92}$ and $Sn_8Co_4C_{88}$ are able to maintain 400 mA h g^{-1} after 40 cycles at 35 mA g^{-1}. The large $CoSn_2$ contribution revealed by Mössbauer spectroscopy in the original and cycled electrodes is responsible for the good electrochemical performance. This interpretation is also supported by impedance spectroscopy measurements.

Introduction

Tin has been regarded as a suitable option to replace graphite in the anode of lithium-ion batteries because of the high Li/Sn ratio known for different intermetallic compounds (up to $Li_{4.4}Sn$). The element is able to deliver specific capacities as high as 994 mA h g^{-1} [1, 2]. Nevertheless, the real application of metallic tin electrodes is restricted by a limited reversibility, which arises from the dramatic volume changes occurring upon cycling [3, 4]. The detrimental contraction–expansion effects can be attenuated by multiple procedures, including the use of glasses and the combination with different elements [5, 6]. More recently, different studies evidenced the advantages of using tin-TM (TM: Ti, V, Cr, Mn, Fe, Ni, Co, and Cu) intermetallic compounds [7, 8]. TM is electrochemically inactive [9, 10], although ternary lithiated phases have been identified in some cases, e.g., for Cu_6Sn_5 [11]. In consequence, a reduction in theoretical capacity is inherent to this approach.

On the other hand, the use of Sn–TM–C composites was found to be an effective way of improving electrode performance [12, 13]. The carbon component forms a stable dispersion matrix, which hinders the agglomeration of intermetallic particles upon cycling. Moreover, carbon provides an electron- and ion-conducting matrix that facilitates the electrochemical reaction with lithium. Also, the ability of carbon materials to reversibly insert lithium contributes positively to the overall reversible capacity. In fact, Sn–TM–C composites are more efficient than their individual components taken separately [14]. In this context, disordered carbons prepared at low temperatures, such as coke, may play an important role. The reduced cost of cokes obtained as a by-product of the petroleum industry is an added value for commercial purposes. Also, low structural ordering leads to large number of different sites for lithium insertion [3].

The intimate mixing of composite components can be carried out by several routes [15–17]. Among others, ball milling has recently attracted more attention in the synthesis of anode materials for lithium-ion batteries based on intermetallic compounds [18–21]. Homogeneous mixtures of ultrafine metal particles embedded in the carbon phase are commonly obtained by mechanical treatments.

F. Nacimiento · P. Lavela (✉) · J. L. Tirado
Laboratorio de Química Inorgánica, Universidad de Córdoba,
Marie Curie,
Campus de Rabanales,
14071 Córdoba, Spain
e-mail: iq1lacap@uco.es

J. M. Jiménez-Mateos
REPSOL,
Ctra. N-Vkm 18,
28930 Móstoles, Madrid, Spain

The aim of this work is to evaluate the validity of a low-cost coke material to act as the carbon source in composites with different Sn/Co and metal/carbon ratios. For this purpose, several Sn–Co–C composites were prepared by ball milling metal oxides and carbon precursors followed by carbothermal reduction. This is a cost-effective procedure for the large-scale production of electrode materials.

Experimental

Sn–Co–C composites were prepared by a two step process. Suitable amounts of commercial SnO_2 (Panreac), CoO (Aldrich), and green coke (REPSOL) were used as precursors of the composite materials. Coke was the only source of the electroactive carbon matrix that embeds the particles of intermetallic compounds in the final composite. The precursors were weighed to prepare a set of samples with different elemental contents. A 15% coke excess was added for balancing the weight loss occurring during carbonization, according to previous reports [14]. The precursors were ground in a planetary ball mill RETSCH S100. The agate jar contained 4 g of precursor material and two 11 g agate balls. The material was ball milled for 5 h at 500 rpm under an air atmosphere. Then, the composite precursors were separated and annealed at 800 °C under a flowing stream of argon (90 mL min^{-1}) for 6 h. The heating rate was 2 °C min^{-1}. Carbon content was analyzed in an Elemental CHNS Analyser *Eurovector EA 3000*, while tin and cobalt contents were determined by EDS. According to their nominal composition, samples will be henceforth referred to as $Sn_{27}Co_{14}C_{59}$, $Sn_7Co_1C_{92}$, $Sn_8Co_4C_{88}$, $Sn_6Co_6C_{88}$, and $Sn_4Co_2C_{94}$.

X-ray diffraction (XRD) patterns were recorded in a Siemens D-5000 apparatus provided with CuKα radiation and graphite monochromator. The 2θ scan rate was 0.04°/1.2 s. Scanning electron microscopy (SEM) images were obtained in a JEOL-SM6300 microscope located at the Research Support Service, University of Córdoba. The ^{119}Sn Mössbauer spectra (MS) were recorded at room temperature with an Ametek–Wissel constant-acceleration spectrometer in transmission mode. The source of radiation was ^{119m}Sn in a $BaSnO_3$ matrix. The isomer shift scale was set by using a $BaSnO_3$ pattern. The peak center of the Sn

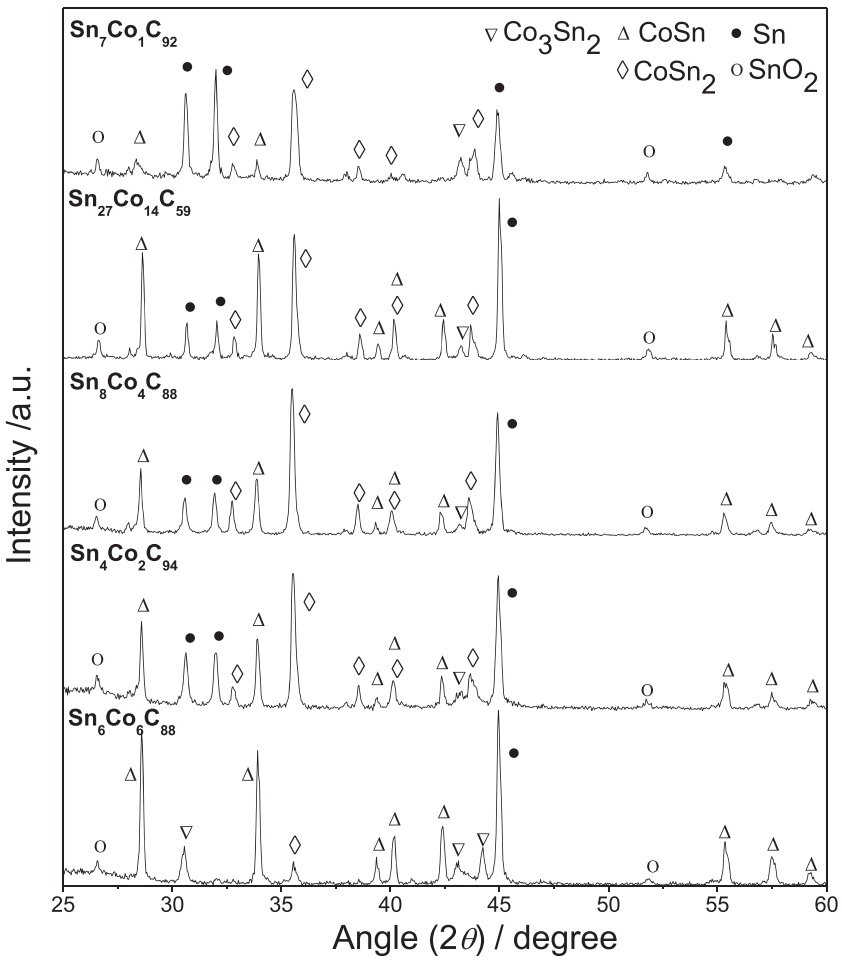

Fig. 1 XRD patterns of Sn–Co–C composites. Indexed phases were marked with *symbols*

(IV) signal was set as the scale zero. The spectra profile was decomposed in Lorentzian lines by using a least-square-based method [22]. The goodness of the fit was controlled by the χ^2 value.

The electrochemical behavior of the Sn–Co–C composites was evaluated by cycling lithium test cells in galvanostatic conditions. The working electrode was prepared by blending active material (60%), carbon black (30%), and PVDF binder (10%). In order to ensure the homogeneous distribution of the polymer binder, *n*-methyl pyrrolidinone was added to form a paste that was spread on a 9-mm cooper disk. The cell assembly was completed with a lithium metal disk of the same diameter as a counter electrode. The electrodes were separated by Whatman glass fiber disks soaked in 1 M $LiPF_6$ (EC/DEC=1:1) electrolyte solution. The cell was finally enclosed in a two-electrode Swagelok™ type cell. The assembly of test cells and handling of the discharged electrodes were carried out in an MBraun glove box under a controlled Ar atmosphere.

An Arbin multichannel galvanostat system was used to cycle lithium cells, with kinetic rates ranging from 35 to 700 mA g^{-1} for both charge and discharge branches. Electrochemical impedance spectroscopy was carried out in an Autolab PGSTAT12 system. Three-electrode lithium cells were used with a lithium metal disk as reference electrode. Before measuring the impedance values, the cells were kept in open circuit for at least 5 h to achieve quasi-equilibrium conditions. An AC voltage signal of 5 mV was applied from 100 kHz to 2 mHz.

Results and discussion

The chemical analysis of the samples revealed high carbon contents, around 90 at.%, except for $Sn_{27}Co_{14}C_{59}$. In the latter composite, lower carbon content was used during the preparation in order to evaluate the influence of the metallic elements in the electrochemical behavior. Concerning the Sn/Co ratio, the chemical analysis showed substantially differing values. Such diversity was also planned during the synthesis in order to determine the effect of Sn/Co ratios on the performance.

Figure 1 shows the XRD patterns of the annealed composites. The short-range ordering of the carbon phase precludes its detection by this technique. Contrarily, a set of narrow reflections can be ascribed to the presence of different crystalline tin-cobalt phases, including tetragonal metallic tin (JCPDS 04-0673), tetragonal $CoSn_2$ (JCPDS 25-0256), Co_3Sn_2 (JCPDS 27-1124), and hexagonal CoSn phase (JCPDS 02-0559). No peaks ascribable to Co_3O_4 were identified. Only minor peaks were assigned to SnO_2 cassiterite (JCPDS 14-1445). The evaluation of the XRD patterns suggests that an efficient carbothermal reduction occurred during the carbonization at 800 °C. Those samples with close Sn/Co ratios ($Sn_{27}Co_{14}C_{59}$, $Sn_8Co_4C_{88}$, and $Sn_4Co_2C_{94}$) were characterized by similar patterns. The diffraction pattern corresponding to $Sn_6Co_6C_{88}$ reveals the major CoSn phase and minor contributions from $CoSn_2$ and Co_3Sn_2. Finally, a significant contribution of metallic tin and $CoSn_2$ is observed for $Sn_7Co_1C_{92}$.

A significant effect of the carbon matrix on the size and morphology of the metallic particles is clearly observed in the SEM micrographs of selected samples (Fig. 2). Thus, samples containing high carbon content showed sub-micrometric metallic particles, embedded in the carbon matrix (Fig. 2b, c). The spherical metallic particles attached to the carbon surface can be assigned to tin. The low

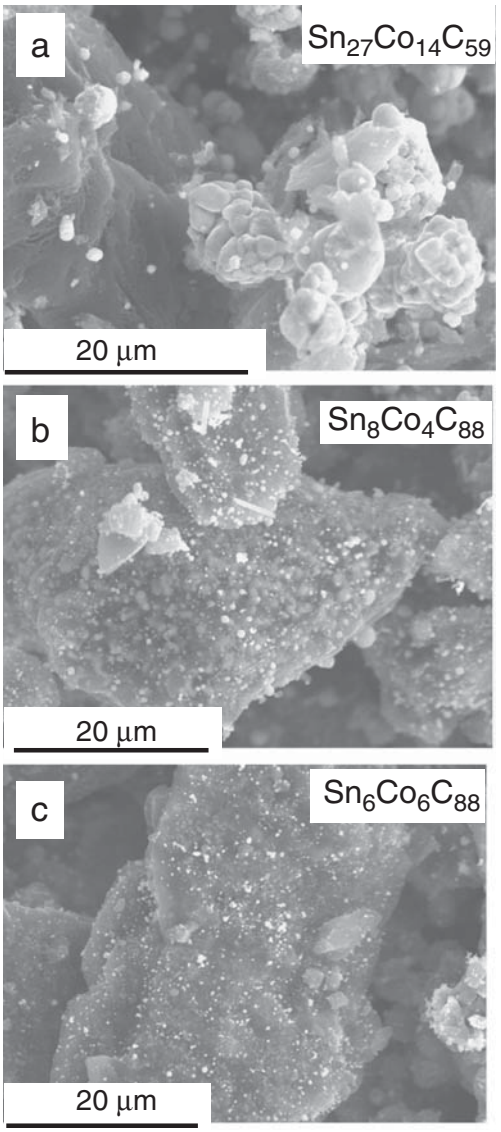

Fig. 2 SEM micrographs of $Sn_{27}Co_{14}C_{59}$, $Sn_8Co_4C_{88}$ and $Sn_6Co_6C_{88}$ composites

melting point of this metal leads to its partial exudation during the carbonization process. These particles appear well dispersed and, most probably firmly attached, on the carbon surface. The exudation effect could be considered as detrimental for the reversibility of the electrochemical reaction. However, previous reports have demonstrated that the use of tin nanoparticles as separated nanowires or nanopillars on the electrode surface provides a suitable morphology that prevents tin agglomeration upon the electrochemical reaction [23, 24]. The sample with low carbon content ($Sn_{27}Co_{14}C_{59}$) revealed large metallic particles of several microns isolated from the carbon phase (Fig. 2a). This particular morphology and phase distribution may have a negative effect on the electrochemical reversibility, as compared with nanodispersed materials.

^{119}Sn Mössbauer spectroscopy is a valuable technique to evaluate the local environment of the probe atom. The spectra of the original composites are shown in Fig. 3. They are characterized by large asymmetric profiles in which the contribution of the distinct Sn–Co phases cannot be visually resolved (Fig. 3). To overcome this problem, the hyperfine parameters of the Co–Sn phases, previously identified by XRD, were taken from the literature and introduced in the fitting procedure to determine their relative contributions. However, slight changes in the hyperfine parameters were allowed in order to achieve a good fitting (Table 1). Recently, it has been demonstrated that the presence of carbon atoms cause an increase in the isomer shift value of the spectrum barycentre as compared with pure tin-cobalt compounds [25]. The quantification of the tin atomic fractions is proportional to the relative contribution to the MS spectrum and the recoil-free fraction. Unfortunately, a complete study of the recoil-free fraction of cobalt-tin compounds is not available in the literature, hence limiting the quantification of tin phases. A Lamb–Mössbauer factor of 0.55was recently reported for CoSn [27]. On the other hand, a factor as low as 0.039 was reported for β-Sn [28].

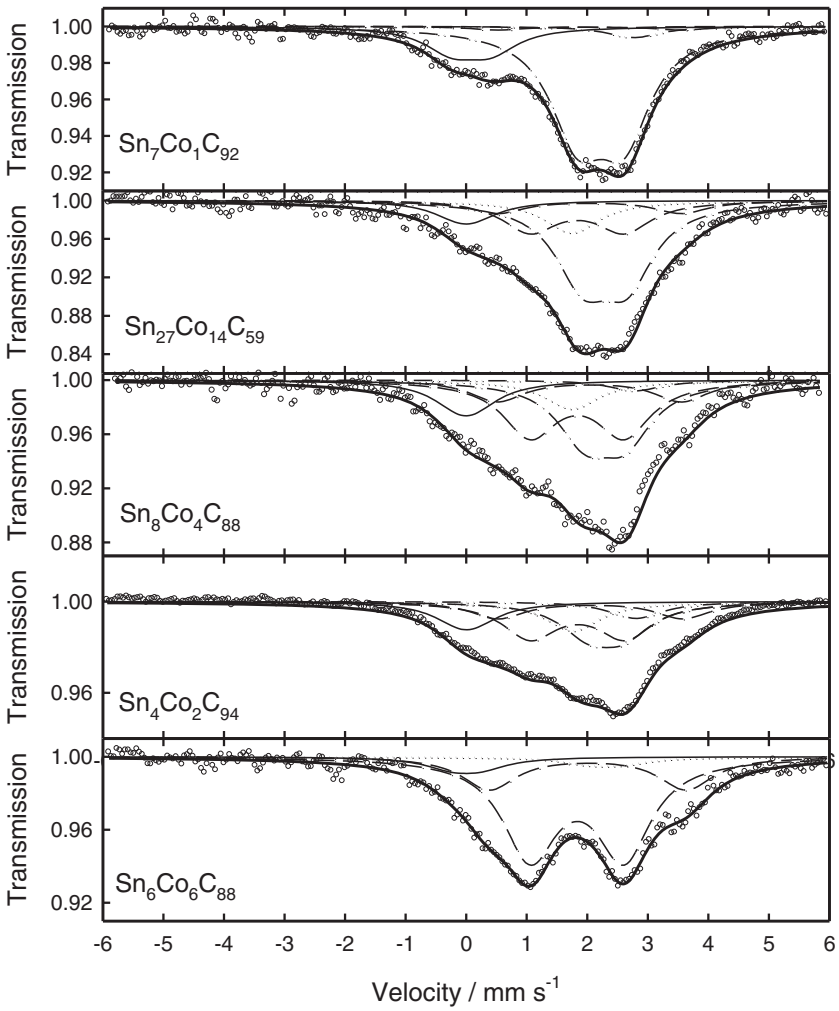

Fig. 3 ^{119}Sn Mössbauer spectra of Sn–Co–C composites. Experimental and fitted spectra are plotted with *symbols* and *lines*, respectively. The decomposed components correspond to SnO_2 (*solid line*), CoSn (*dashed line*), $CoSn_2$ (*dashed-dotted line*), β-Sn (*dashed-dotted-dotted-dashed line*), and Co_3Sn_2 (*dotted line*)

Table 1 Hyperfine parameters of fitted Mössbauer spectra of Sn–Co–C composites

Sample	s/d	Tin phase	δ (mm/s)	Δ (mm/s)	Γ (mm/s)	C (%)	χ^2
$Sn_7Co_1C_{92}$	s	β-Sn	2.76 (2)		1.084 (8)	4.23	0.601
	d	CoSn	1.82 (3)	1.542 (3)	1.084 (8)	0.92	
	d		2.02 (3)	3.025 (7)	1.084 (8)	2.7	
	d	$CoSn_2$	2.22 (2)	0.77 (1)	1.084 (8)	75.09	
	d	SnO_2	0.08 (6)	0.64 (7)	1.084 (8)	17.06	
$Sn_{27}Co_{14}C_{59}$	d	CoSn	1.83 (4)	1.549 (3)	1.089 (7)	21.03	0.556
	d		2.03 (2)	3.038 (7)	1.089 (7)	8.86	
	d	$CoSn_2$	2.29 (1)	0.73 (2)	1.089 (7)	50.38	
	s	Co_3Sn_2	1.739 (3)		1.089 (7)	11.18	
	d	SnO_2	0.001 (3)	0.242 (1)	1.089 (7)	8.55	
$Sn_8Co_4C_{88}$	s	β-Sn	2.78 (1)		1.089 (7)	3.21	0.649
	d	CoSn	1.81 (4)	1.549 (3)	1.089 (7)	32.18	
	d		2.05 (5)	3.038 (7)	1.089 (1)	12.7	
	d	$CoSn_2$	2.29 (7)	0.6 (1)	1.089 (7)	32.09	
	s	Co_3Sn_2	1.74 (2)		1.089 (7)	8.59	
	d	SnO_2	0.001 (8)	0.242 (1)	1.089 (7)	11.23	
$Sn_4Co_2C_{94}$	s	β-Sn	2.80 (3)		1.095 (6)	7.04	0.762
	d	CoSn	1.847 (8)	1.558 (3)	1.095 (6)	29.65	
	d		2.05 (2)	3.055 (7)	1.095 (6)	14.12	
	d	$CoSn_2$	2.31 (4)	0.58 (7)	1.095 (6)	24.62	
	s	Co_3Sn_2	1.753 (7)		1.095 (6)	12.19	
	d	SnO_2	0.00 (1)	0.243 (1)	1.095 (6)	12.37	
$Sn_6Co_6C_{88}$	d	CoSn	1.83 (1)	1.55 (2)	1.088 (9)	66.78	0.556
	d		2.00 (5)	3.25 (9)	1.088 (9)	22.27	
	d	$CoSn_2$	2.292 (3)	0.572 (1)	1.088 (9)	4.13	
	d	SnO_2	0.001 (4)	0.50 (9)	1.088 (9)	6.82	
Hyperfine parameters from the literature [25, 26]	s	β-Sn	2.559 (3)		1.022 (9)	100	
	d	CoSn	1.854 (6)	1.60 (1)	0.99 (1)	67	0.97
	d		2.03 (1)	3.14 (2)	0.99 (2)	33	
	s	$CoSn_2$	2.14	0.78			
	d	Co_3Sn_2	1.74	1.3		100	
	d	SnO_2	−0.011	0.65	1.27	100	0.48

s/d singlet (*s*) or doublet (*d*), δ isomeric shift, Δ quadrupole splitting, Γ line-width at half maximum, C relative contribution, χ^2 goodness of the fitting

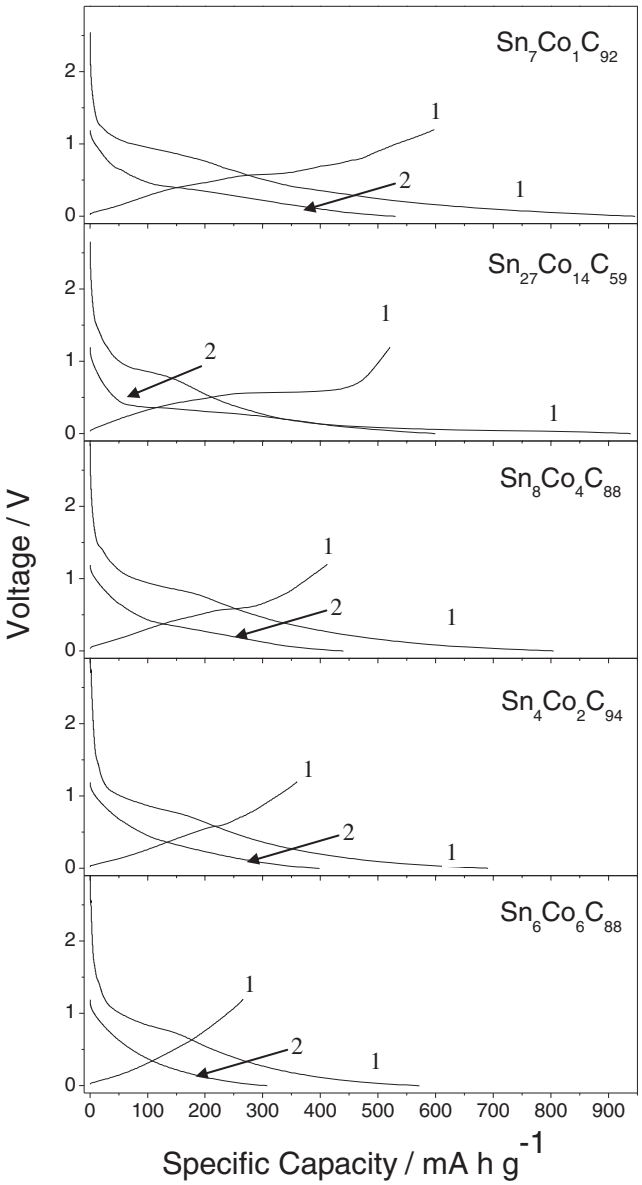

Fig. 4 Voltage versus capacity plots of Sn–Co–C composites for the first discharge and charge and second discharge. Lithium cells were cycled at 35 mA g^{-1}

The marked difference between these values explains the low contribution of β-Sn to the Mössbauer spectra, as compared with XRD patterns.

Figure 4 shows the voltage vs. capacity plots for the first cycle and second discharge of lithium test cells using the metal–carbon composites as working electrodes. The first discharge evidences a large capacity which is not recovered after subsequent charge. This phenomenon is commonly ascribed to the irreversibility of the quasi-plateau observed at 0.8–1 V, which is attributed to the formation of the solid-electrolyte interface that impedes further electrolyte decomposition [29]. Below 0.5 V, a sloping voltage extends for several hundreds of mA h g^{-1}. A good reversibility of this effect is observed on further cycling and is attributed to both the reversible formation of Li–Sn intermetallic compounds and the insertion of lithium in the carbon matrix [1, 2, 22]. According to the theoretical capacity of carbon and tin, electrochemical reactions of the composite with lithium can be summarized as:

$$Li + 6\ C \rightleftarrows LiC_6 \quad (1)$$

$$4.4\ Li + Sn \rightleftarrows Li_{4.4}Sn \quad (2)$$

According to these reactions, a maximum $Li_{46}Sn_7Co_1C_{92}$ nominal stoichiometry could be reached, that can be converted to 618 mA h g^{-1}. The experimental capacity

value recorded for this sample after the first discharge is higher than the theoretical value. However, it is well known that the disordered structure of coke provides additional sites for lithium insertion. The resulting capacity values are significantly higher than those found when lithium is exclusively hosted in the interlayer space of the grapheme layers. Moreover, the Sn–Co or Sn–Co–C interactions may involve an additional contribution to the electrochemical process which justifies a deeper analysis.

Large capacities were observed for $Sn_{27}Co_{14}C_{59}$ and $Sn_7Co_1C_{92}$. In the former sample, the high metal content may explain this behavior, while for $Sn_7Co_1C_{92}$ the high contribution of $CoSn_2$ is responsible for the good performance. The high Sn/Co ratio in the $CoSn_2$ stoichiometry would justify a high theoretical capacity and hence a positive contribution to the overall capacity of the composite. Concerning CoSn and Co_3Sn_2, different cell performances can be found in the literature. Thus, Zhang et al. reported that CoSn and Co_3Sn_2 intermetallics did not completely convert to the Li_xSn during the first discharge while $CoSn_2$ is able to reach full lithiation [30]. Xie et al. have reported capacity fading in microcrystalline Co_3Sn_2. It was ascribed to a crystallization process during cycling [31]. On the contrary, nanocrystalline Co_3Sn_2 shows capacities around 450 mA h g^{-1} and good capacity retention at different rates [32]. For nanocrystalline CoSn, the reaction with lithium produces a reversible amorphization of the intermetallic compound. The presence of Co atoms avoids the formation of crystalline phases of Li_xSn [33]. These differences imply that, together with composition, both crystallinity and particle morphology play an important role. Concerning the possible effect of Sn–Co–C interactions on the electrochemical response vs. lithium, the addition of both Co and C was envisaged as a way to stabilize the structure during the repeated reaction with lithium [34].

Lithium cells were galvanostatically cycled in order to evaluate capacity retention in the composite electrodes (Fig. 5). For the carbonized coke, the capacity was initially high. However, an enhanced capacity fading was observed during the first few cycles. Thus, the separate contribution of the carbon matrix to the electrochemical performance must be considered as having a secondary role. On the contrary, the effect of carbon matrix on capacity retention in the composites is clearly evidenced for $Sn_{27}Co_{14}C_{59}$ sample. Thus, the high metal/carbon ratio for this sample can be considered the origin of the enhanced capacity fading, as found in pure tin electrodes [3, 4].

The differential capacity curves for $Sn_{27}Co_{14}C_{59}$ and $Sn_8Co_4C_{88}$ showed important differences between samples with different carbon content. Thus, the charging curves for $Sn_{27}Co_{14}C_{59}$ are characterized by an intense peak at 0.58 V which is shifted to 0.60 V while its intensity is diminished

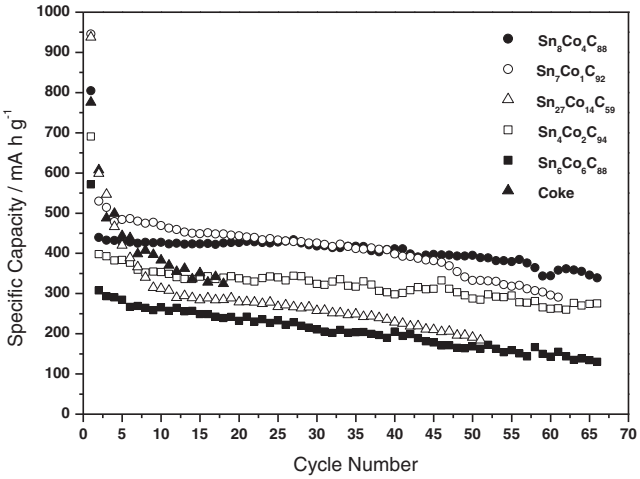

Fig. 5 Galvanostatic cycling of Sn–Co–C composites at 35 mA g^{-1}

(Fig. 6). This behavior has been ascribed to the occurrence of microcrystalline $CoSn_2$ with detrimental effect on the lithium cell cycling. On the contrary, $Sn_8Co_4C_{88}$ revealed a cathodic peak at 0.6 V which remained basically unmodified after five cycles. A similar behavior was observed in nanocrystalline $CoSn_2$ and correlated to good capacity retention on prolonged cycling [35].

It is well known that the metallic particles detached from the carbonaceous phase (Fig. 2a) are more prone to suffer

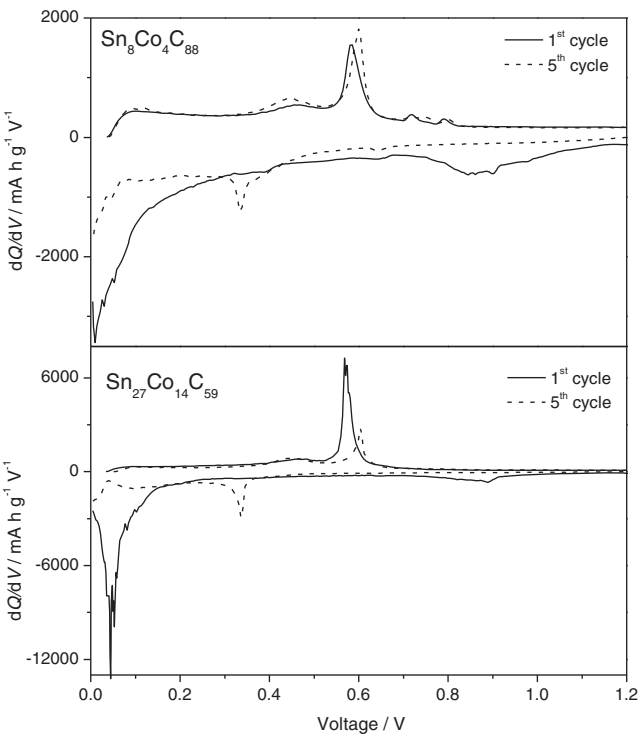

Fig. 6 Differential capacity plots for $Sn_{27}Co_{14}C_{59}$ and $Sn_8Co_4C_{88}$ after one and five cycles

particle aggregation, which leads to electrode degradation [4]. However, a large capacity fading was also observed for $Sn_6Co_6C_{88}$, despite of its high carbon content. It means that additional factors must be considered. Irrespective of their similar Sn/Co ratios, $Sn_8Co_4C_{88}$, $Sn_{27}Co_{14}C_{59}$, and $Sn_4Co_2C_{94}$ show distinct cycling performances. This behavior evidences that the metal/carbon ratio has more influence on the electrochemical response. Dahn et al. have evaluated a wide variety of $Sn_{1-x}Co_x$ compounds. A plot of specific capacity vs. Co atomic percent showed a nonlinear behavior and an enhanced decrease of capacity for low Sn/Co ratios [34]. Thus, the low Sn/Co ratios favoring the presence of less reactive CoSn and Co_3Sn_2 is detrimental as compared with large $CoSn_2$ contributions [30]. Capacity values of 400 mA h g^{-1} at 35 mA g^{-1} were recorded after 40 cycles. This electrochemical behavior is also reflected in the different capability of the electrodes to retain suitable capacity values at high C rates (Fig. 7). These results show that $Sn_7Co_1C_{92}$ and $Sn_8Co_4C_{88}$ are able to maintain 300 mA h g^{-1} at 2 °C after 28 cycles. In contrast, capacity values as low as 203 mA h g^{-1} were recorded at 2°C for $Sn_6Co_6C_{88}$.

Electrochemical impedance spectroscopy allows an evaluation of the internal resistance at the working electrode/electrolyte interphase, which plays a significant role in lithium migration. Figure 8a displays the Nyquist plots of selected samples, chosen in the basis of their different composition and electrochemical behavior. The spectra were fitted according to an equivalent circuit commonly reported in the literature for carbonaceous materials (Fig. 8b) [36, 37]. RE refers to the resistance of the electrolyte. Two depressed semicircles at high and intermediate frequencies are commonly attributed to the kinetic limitations to lithium migration through the solid-electrolyte interface (SEI) and the charge transfer at the electrode surface. These phenomena are interpreted in terms of a resistance and a constant phase element (CPE) placed in parallel in the equivalent circuit (R_{SEI}, CPE_{SEI}), (R_{CT},

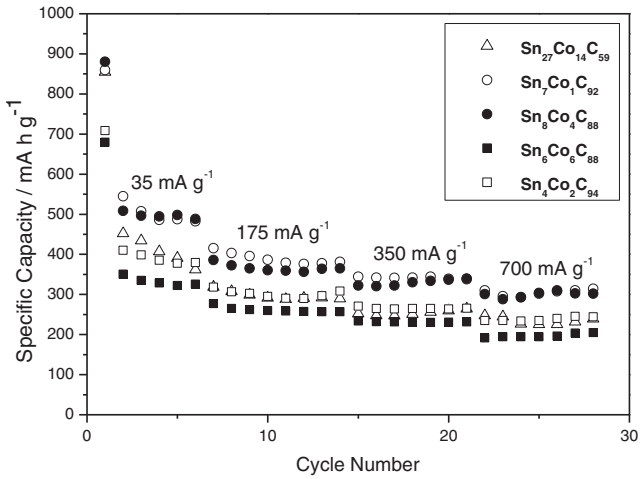

Fig. 7 Galvanostatic cycling of Sn–Co–C composites at different kinetic rates

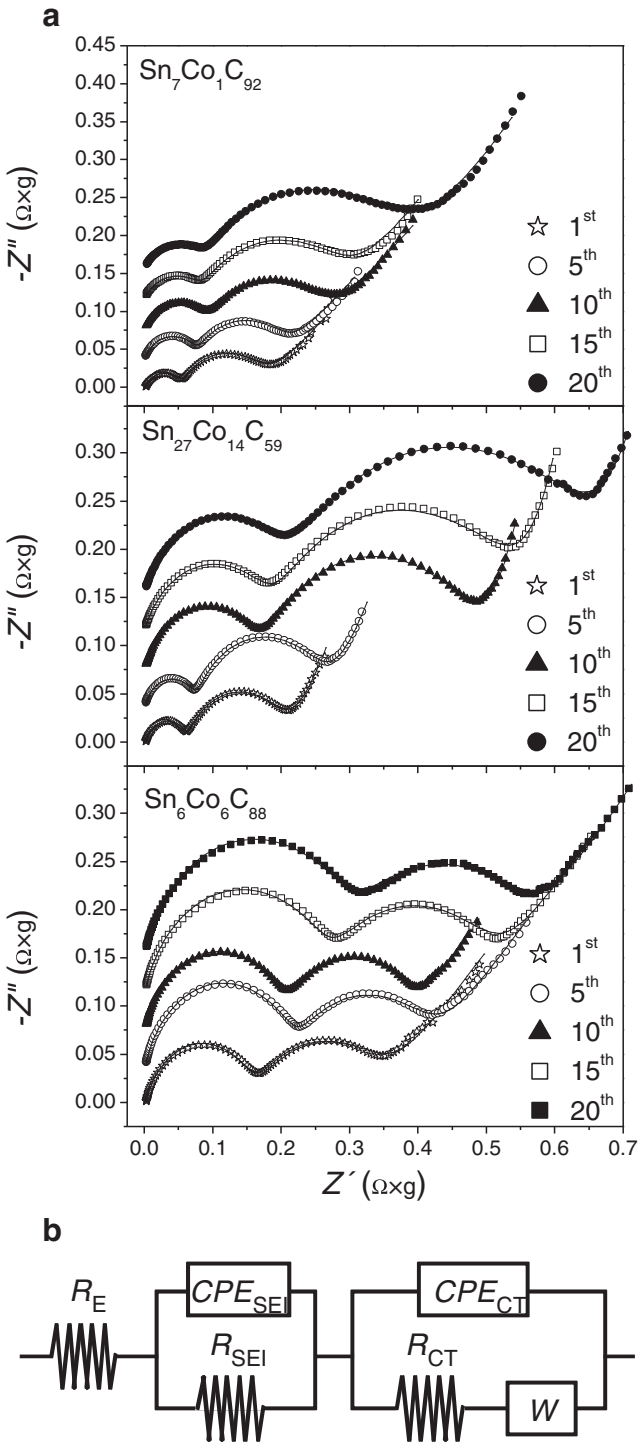

Fig. 8 **a** Nyquist plots of fully discharged electrodes after several cycles. Experimental data are plotted as symbols and the fitted spectra as lines. **b** Equivalent circuit used for the fitting of the spectra

Table 2 Electrical resistance of selected Sn–Co–C composites as calculated by fitting their impedance spectra

Sample	Resistance/Ω×g	1 discharge	5 discharge	10 discharge	15 discharge	20 discharge
$Sn_7Co_1C_{92}$	R_{SEI}	0.0535	0.0766	0.0932	0.0826	0.0865
	R_{CT}	0.1233	0.1292	0.1618	0.2056	0.2880
$Sn_{27}Co_{14}C_{59}$	R_{SEI}	0.062	0.0742	0.1708	0.1843	0.2092
	R_{CT}	0.1329	0.1863	0.3147	0.3589	0.4486
$Sn_6Co_6C_{88}$	R_{SEI}	0.1562	0.2180	0.2034	0.2675	0.2974
	R_{CT}	0.1919	0.1978	0.1868	0.2412	0.2649

CPE_{CT}). In addition, the line observed at low frequencies is ascribed to lithium diffusion into the electrode material and is fitted to a Warburg element (*W*) [37, 38]. The resulting resistance values are listed in Table 2. The values of solid-electrolyte interphase resistance (R_{SEI}) were generally of lower magnitude than charge transfer resistances (R_{CT}). For sample $Sn_7Co_1C_{92}$, the R_{SEI} values were low and tended to stabilize at ca. 0.08 Ω×g after 20 cycles. In contrast, resistance values higher than 0.2 Ω×g were recorded for $Sn_6Co_6C_{88}$ and $Sn_{27}Co_{14}C_{59}$. Concerning R_{CT} values, a marked increase on cycling was observed for $Sn_{27}Co_{14}C_{59}$, while the other samples reflect the beneficial effect of the carbon matrix to provide a stable and conductive electrode–electrolyte interphase. Considering both contributions, sample $Sn_7Co_1C_{92}$ has the lower overall resistance values upon 20 cycles. It can be correlated with the higher capacity values retained by this sample after 20 cycles, as shown in Fig. 5.

Ex situ XRD and ^{119}Sn Mössbauer measurements were recorded on cycled electrodes to unveil changes in the intermetallic phases upon cycling. Figure 9 shows the ex situ XRD patterns of $Sn_7Co_1C_{92}$ electrodes after one discharge and after one and five cycles. The discharged electrode revealed the effective Li–Sn alloy formation by the presence of Li_5Sn_2 (JCPDS 29-0839) and $Li_{13}Sn_5$ (JCPDS 29-0838). This fact was also confirmed by ^{119}Sn Mössbauer spectroscopy (Fig. 10). A split signal was observed for the discharged electrode, with the centroid isomer shift value located close to those reported for crystalline $Li_{13}Sn_5$ and Li_5Sn_2 [39]. Most probably, Li_xSn phases are the products of the electrochemical reaction of tin metal component in the composite material. Recently, it was demonstrated that pure nanodispersed $CoSn_2$ does not show the typical anodic peak commonly ascribed to the formation of Li_xSn phases [40]. On further charge, a large number of reflections could be indexed to Sn, CoSn, $CoSn_2$, and $Li_{13}Sn_5$ (Fig. 9). The presence of tin-cobalt compounds support the reversibility of the electrochemical reaction of lithium with $CoSn_2$. Nevertheless, the presence of minor Li–Sn phases is also visible. It can be assigned to the limited lithium diffusion at the selected charging rate and/or to particle isolation into the composite material. ^{119}Sn Mössbauer spectra of cycled electrodes are characterized by asymmetric profiles in which most of the components are overlapped. For this reason, the existing phases were determined from the XRD patterns depicted in Fig. 8. Then, their hyperfine parameters were fixed in the fitting process and only their relative contributions were allowed to change (Table 3). The highest contribution corresponded to $CoSn_2$, although a significant increase of CoSn was detected as compared with the original composite, which evidenced a partial recovery of the cobalt-tin intermetallic compound after charging, as found in nanocrystalline CoSn alone [33]. The presence of residual $Li_{13}Sn_5$ was less pronounced for the fifth charge and may involve an enhanced cycling efficiency after the first cycle, in agreement with the capacity fading observed during the first cycles. Finally, the increase in β-tin contribution on cycling can be explained in terms of a degradation of the cobalt-tin linkage during cycling.

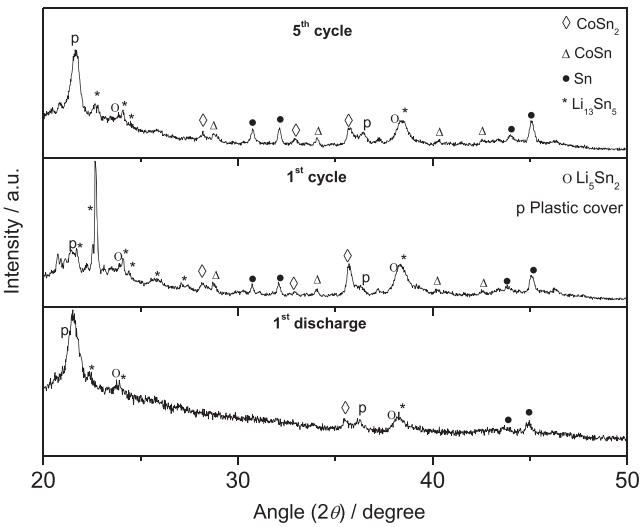

Fig. 9 XRD patterns of $Sn_7Co_1C_{92}$ electrodes after one disk, one, and five cycles in lithium cells. Indexed phases were marked with *symbols*

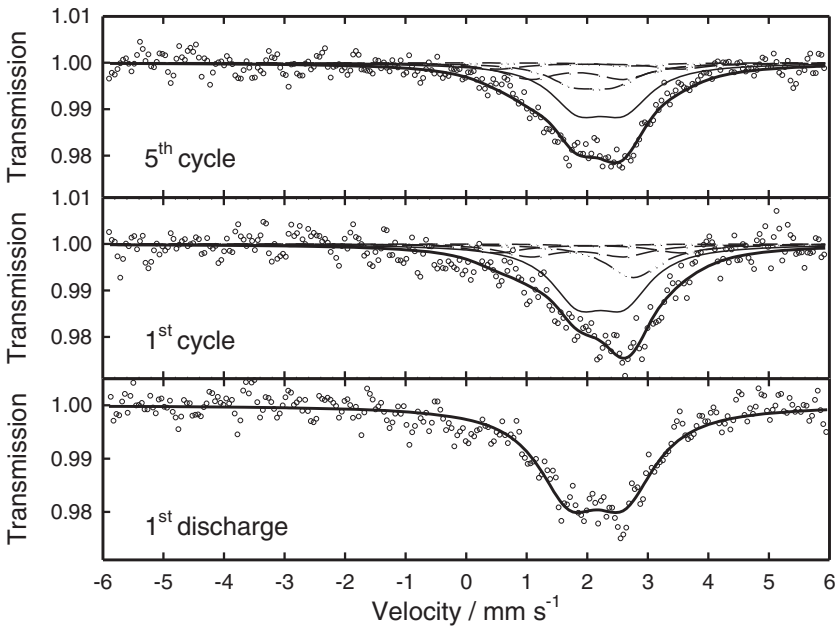

Fig. 10 ^{119}Sn Mössbauer spectra of $Sn_7Co_1C_{92}$ electrodes after one discharge, one, and five cycles in lithium cells. Experimental and fitted spectra are plotted with symbols, and lines, respectively. The decomposed components correspond to $Li_{13}Sn_5$ (*solid line*), CoSn (*dashed line*), $CoSn_2$ (*dashed-dotted line*), β-Sn (*dashed-dotted-dotted-dashed line*) and Co_3Sn_2 (*dotted line*)

Conclusions

Sn–Co–C composites were prepared by the carbothermal reaction of precursors containing a green coke and tin and cobalt oxides. The homogeneity of the resulting product was assured by ball milling the precursor mixture before the carbonization under Ar atmosphere. Samples with different carbon and metal content were produced. The XRD and ^{119}Sn Mössbauer spectroscopy of the original composites revealed the prevalence of Sn and $CoSn_2$ phases for those samples prepared with a high Sn/Co ratio. SEM images showed a homogeneous dispersion of sub-micrometric metallic particles in the carbon matrix. In contrast, large isolated metallic grains were present in the sample with the lowest carbon content.

Galvanostatic cycling at several kinetic rates revealed that $Sn_7Co_1C_{92}$ and $Sn_8Co_4C_{88}$ are able to maintain 400 mA h g^{-1} at 35 mA g^{-1} after 40 cycles. A major $CoSn_2$ contribution, revealed by Mössbauer spectroscopy, could be correlated with a good electrochemical performance in these composites. These results are supported by the low internal impedance measured in $Sn_7Co_1C_{92}$ electrodes after several discharges.

A more detailed analysis of discharged and cycled electrodes of $Sn_7Co_1C_{92}$ by XRD and Mössbauer spectroscopy allowed to conclude that the presence of non-oxidized $Li_{13}Sn_5$ arising from metallic tin may contribute to the undesirable irreversibility of the first cycle. However, after five cycles, the contribution of $CoSn_2$ remained significant while $Li_{13}Sn_5$ almost disappeared,

Table 3 Hyperfine parameters of fitted Mössbauer spectra of $Sn_7Co_1C_{92}$ cycled electrodes

$Sn_7Co_1C_{92}$	s/d	Tin phase	δ (mm/s)	Δ (mm/s)	Γ (mm/s)	C (%)	χ^2
1st discharge	d	$Li_{13}Sn_5$	2.16 (3)	0.91 (5)	1.272	100.0	0.531
1st cycle	d	CoSn	1.82 (3)	1.542 (3)	1.084 (8)	18.9	0.400
	d		2.02 (3)	3.025 (7)	1.084 (8)	7.79	
	d	$CoSn_2$	2.22 (2)	0.77 (1)	1.084 (8)	49.98	
	s	β-Sn	2.76 (2)	–	1.084 (8)	2.0	
	d	$Li_{13}Sn_5$	2.16 (3)	0.91 (5)	1.084 (8)	21.33	
5th cycle	s	β-Sn	2.76 (2)	–	1.084 (8)	19.12	0.619
	d	CoSn	1.82 (3)	1.542 (3)	1.084 (8)	13.33	
	d		2.02 (3)	3.025 (7)	1.084 (8)	9.78	
	d	$CoSn_2$	2.22 (2)	0.77 (1)	1.084 (8)	56.51	
	d	$Li_{13}Sn_5$	2.16 (3)	0.91 (5)	1.084 (8)	1.26	

s/d singlet (*s*) or doublet (*d*), δ isomeric shift, Δ quadrupole splitting, Γ line-width at half maximum, C relative contribution, χ^2 goodness of the fitting

thus explaining the better capacity retention observed in subsequent cycles.

Acknowledgments The authors are grateful to MEC (Contract PET2005_0670_01) and MICINN (MAT2008-05880) for financial support. We also thank to the Central Services of the University of Córdoba, and especially to F. Gracia for the use of the SEM microscope. F. Nacimiento is indebted to MEC for his predoctoral grant.

References

1. Winter M, Besenhard JO (1999) Electrochim Acta 45:31–50
2. Tirado JL (2003) Mater Sci Eng R 40:103–136
3. Winter M, Besenhard JO, Michael E (1998) Adv Mater 10: 725–763
4. Beaulieu LY, Eberman KW, Turner RL, Krause JL, Dahn JR (2001) Electrochem Solid-State Lett 4:A137–A140
5. Idota Y, Kubota T, Matsufuji A, Maekawa Y, Miyasaka T (1997) Science 276:1395–1397
6. Alcántara R, Fernández-Madrigal FJ, Lavela P, Tirado JL, Jumas JC, Olivier-Fourcade J (1999) J Mater Chem 9:2517–2521
7. Aboulaich A, Mouyane M, Robert F, Lippens PE, Olivier-Fourcade J, Willmann P, Jumas JC (2007) J Power Sources 174:1224–1228
8. Todd ADW, Mar RE, Dahn JR (2006) J Electrochem Soc 153: A1998–A2005
9. Mao O, Dunlap RA, Courtney IA, Dahn JR (1998) J Electrochem Soc 145:4195–4202
10. Ionica-Bousquet CM, Lippens PE, Aldon L, Olivier-Fourcade J, Jumas JC (2006) Chem Mater 18:6442–6447
11. Choi W, Lee JY, Lim HS (2004) Electrochem Commun 6:816–820
12. Inoue H Proceedings of the International Meeting on Lithium Batteries. The Electrochemical Society, Biarritz, France
13. Lee SI, Yoon S, Park CM, Lee JM, Kim H, Im D, Doo SG, Sohn HJ (2008) Electrochim Acta 54:364–369
14. Tirado JL, Santamaría R, Ortiz GF, Menéndez R, Lavela P, Jiménez-Mateos JM, Gómez García FJ, Concheso A, Alcántara R (2007) Carbon 45:1396–1409
15. Hassoun J, Ochal P, Panero S, Mulas G, Bonatto Minella C, Scrosati B (2008) J Power Sources 180:568–575
16. Ferguson PP, Todd ADW, Dahn JR (2008) Electrochem Commun 10:25–31
17. Fan XY, Ke FS, Wei GZ, Huang L, Sun SG (2009) J Solid State Electrochem 13:1849–1858
18. Zhongxue C, Jiangfeng Q, Xinping A, Yuliang C, Hanxi Y (2009) J Power Sources 189:730–732
19. Mulas G, Enzo S, Bonatto-Minella C, Arca E, Gerbaldi C, Penazzi N, Bodoardo S, Hassoun J, Panero S (2009) J Solid State Electrochem 13:239–243
20. Liang Y, Liu Y, Jia ZJ (2009) J Alloys Compd 474:590–594
21. Lee KM, Lee YS, Kim YW, Sun YK, Lee SM (2009) J Alloys Compd 472:461–465
22. Kündig W (1969) Nucl Instr Methods 75:336–340
23. Li N, Martin CR, Scrosati B (2001) J Power Sources 97–98: 240–243
24. Ortiz GF, Hanzu I, Lavela P, Knauth P, Tirado JL, Djenizian T (2010) Chem Mater 22:1926–1932
25. Ortiz G, Alcántara R, Rodríguez I, Tirado JL (2007) J Electroanal Chem 605:98–108
26. Jaen J, Varsanyi ML, Kovacs E, Czako-Nagy I, Buzas A, Vertes A, Kiss L (1984) Electrochim Acta 29:1119–1122
27. Alcántara R, Lavela P, Ortiz G, Rodríguez I, Tirado JL (2008) Hyperfine Interact 187:13–17
28. Greenwood NN, Gibb TC (1971) Mössbauer spectroscopy. Chapman & Hall, London
29. Fong R, Sacken UV, Dahn JR (1990) J Electrochem Soc 137:2009–2013
30. Zhang JJ, Xia YY (2006) J Electrochem Soc 153:A1466–A1471
31. Xie J, Zhao XB, Cao GS, Tu JP (2007) J Power Sources 164:386–389
32. Alcántara R, Ortiz G, Rodríguez I, Tirado JL (2009) J Power Sources 189:309–314
33. Alcántara R, Rodríguez I, Tirado JL (2008) ChemPhysChem 9:1171–1177
34. Dahn JR, Mar RE, Abouzeid A (2006) J Electrochem Soc 153: A361–A365
35. Alcántara R, Nwokeke UG, Nacimiento F, Lavela P, Tirado JL Proceedings of the SPIE Defense, Security, and Sensing Conferences. Abstract no 8035-05 2011 Orlando, USA
36. Funabiki A, Inaba M, Ogumi Z, Yuasa S, Otsuji J, Tasaka A (1998) J Electrochem Soc 145:172–178
37. Wang C, Appleby AJ, Little FE (2002) J Electrochem Soc 149: A754–A760
38. Aurbach D, Gnanaraj JS, Levi MD, Levi EA, Fischer JE, Claye A (2001) J Power Sources 97:92–96
39. Dunlap RA, Small DA, MacNeil DD, Obrovac NN, Dahn JR (1999) J Alloys Compd 289:135–142
40. Nacimiento F, Alcántara R, Tirado JL (2009) J Alloys Compd 485:385–390